

Surface Flows From Magnetograms

B. T. Welsch¹ and G. H. Fisher¹

Abstract. Estimates of velocities from time series of photospheric and/or chromospheric vector magnetograms can be used to determine fluxes of magnetic energy (the Poynting flux) and helicity across the magnetogram layer, and to provide time-dependent boundary conditions for data-driven simulations of the solar atmosphere above this layer. Velocity components perpendicular to the magnetic field are necessary both to compute these transport rates and to derive model boundary conditions. Here, we discuss some possible approaches to estimating perpendicular flows from magnetograms. Since Doppler shifts contain contributions from flows parallel to the magnetic field, perpendicular velocities are not generally recoverable from Doppler shifts alone. The induction equation’s vertical component relates evolution in B_z to the perpendicular flow field, but has a finite null space, meaning some “null” flows, e.g., motions along contours of normal field, do not affect B_z . Consequently, additional information is required to accurately specify the perpendicular flow field. Tracking methods, which analyze $\partial_t B_z$ in a neighborhood, have a long heritage, but other approaches have recently been developed. In a recent paper, several such techniques were tested using synthetic magnetograms from MHD simulations. Here, we use the same test data to characterize: 1) the ability of the induction equation’s normal component, by itself, to estimate flows; and 2) a tracking method’s ability to recover flow components that are perpendicular to \mathbf{B} and parallel to contours of B_z . This work has been supported by NASA Heliophysics Theory grant NNG05G144G.

1. Why study surface flows from magnetograms?

The large length scales and relatively high conductivity of the plasma in the solar corona imply that, to a good approximation, magnetic flux is frozen to the plasma there. Consequently, the coronal magnetic field is “line-tied” to the plasma in lower atmospheric layers where hydrodynamic forces can be stronger than Lorentz forces — the photosphere and lower chromosphere — and coronal evolution is strongly coupled to evolution in these layers. Accordingly, observations of magnetic field evolution below the Sun’s corona — typically, sequences of photospheric or chromospheric magnetograms — provide crucial tools understand coronal evolution.

Usually, vector magnetograms are more useful than line-of-sight (LOS) magnetograms for studying coronal evolution, because information derived from LOS measurements alone will not, in general, be consistent with the actual magnetic field, which has field components both parallel and transverse to the LOS. Although time series of vector magnetograms have historically been rare, SOLIS

¹Space Sciences Laboratory, University of California, 7 Gauss Way, Berkeley, CA 94720-7450

(Henney *et al.* 2002), the Solar Optical Telescope (SOT, Tarbell 2006) on Hinode, and the Solar Dynamics Observatory’s Helioseismic and Magnetic Imager (HMI) (Scherrer and The HMI TEAM 2005), should dramatically improve photospheric vector magnetogram spatial and temporal coverage in the near future.

Several techniques have been developed to derive flows from time series of magnetograms (Chae 2001; Kusano *et al.* 2002; Welsch *et al.* 2004; Longcope 2004; Georgoulis and LaBonte 2006; Schuck 2006). Estimated flows at the base of the corona can be used to derive the fluxes of magnetic helicity, energy, and free energy into the corona, (Démoulin and Berger 2003; Pariat *et al.* 2005; Welsch 2006). Further, flow estimates can be used to provide time-dependent boundary conditions for data-driven simulations of coronal magnetic field evolution.

This paper briefly reviews progress on estimating surface flows from magnetogram sequences, and demonstrates some aspects of the problem with test data.

2. Progress in estimating surface flows from magnetograms

How have velocities been derived from vector magnetograms? Chae (2001) applied local correlation tracking (LCT) (November and Simon 1988) to LOS photospheric magnetograms to determine the proper motions of magnetic features on the magnetogram surface, and assumed the inferred flows $\mathbf{u}^{(\text{LCT})}$ were estimates of the horizontal plasma velocities \mathbf{v}_h . (Here the h subscript denotes a vector’s components tangential to the magnetogram surface. We avoid the subscript t , which has been used to refer to vector components both transverse to the LOS and tangential to the solar surface.) Assuming that the observed evolution of the photospheric magnetic field is governed by flows according to the ideal induction equation,

$$\frac{\partial \mathbf{B}}{\partial t} = -c(\nabla \times \mathbf{E}) = \nabla \times (\mathbf{v} \times \mathbf{B}), \quad (1)$$

Kusano *et al.* (2002) proposed using the component of equation (1) normal to the magnetogram,

$$\frac{\partial B_z}{\partial t} = \hat{\mathbf{z}} \cdot \nabla \times (\mathbf{v} \times \mathbf{B}) = -\nabla \cdot (\mathbf{v}_h B_z - v_z \mathbf{B}_h), \quad (2)$$

to derive three-component velocity fields — v_x, v_y, v_z . Here, we have defined the magnetogram surface to be the horizontal plane containing $\hat{\mathbf{x}}$ and $\hat{\mathbf{y}}$, with a vertical normal $\hat{\mathbf{z}}$. The three components of \mathbf{v} cannot completely determined from (2) alone, so more data or assumptions are required to close the system for \mathbf{v} .

What about the horizontal components of equation (1)? As Kusano *et al.* (2002) noted, only the normal component of equation (1) is completely specified by vector magnetic field measurements from a single atmospheric layer; the other components of equation (1) contain vertical derivatives of horizontal magnetic field components, and therefore require measurements of the vector magnetic field at a different height in the atmosphere (e.g., the chromosphere) which are only rarely available (Leka and Metcalf 2003; Metcalf *et al.* 2005).

Kusano *et al.* (2002) assumed LCT velocities, \mathbf{u} , to be equivalent to \mathbf{v}_h to close the system. Démoulin and Berger (2003) argued that tracked motions of magnetic flux on the solar photosphere, \mathbf{u} , result from the combined effects of horizontal plasma velocities transporting vertical magnetic fields and vertical plasma velocities transporting horizontal magnetic fields, via

$$\mathbf{u}B_z = \mathbf{v}_h B_z - v_z \mathbf{B}_h . \quad (3)$$

The distinction between apparent motions of flux and plasma velocities led Welsch (2006) to term \mathbf{u} the “flux transport velocity.” Démoulin and Berger (2003) suggested that LCT could be used to infer \mathbf{u} , but not \mathbf{v}_h directly. We note that, in addition to ideal flux transport, diffusive effects can also lead to apparent flux transport velocities (Welsch 2006), although we ignore these effects in the present work.

Since the seminal work of Kusano *et al.* (2002), still more techniques have been developed that determine velocities from vector magnetograms. Welsch *et al.* (2004) used equation (3) to combine Fourier LCT (FLCT) results with equation (2) to determine a photospheric flow field in a method they termed inductive local correlation tracking, or ILCT. Longcope (2004) developed the minimum energy fit (MEF), which finds the photospheric velocity field that is strictly consistent with equation (2) and that minimizes a penalty function, e.g., the integrated square of the three-component photospheric velocity. Georgoulis and LaBonte (2006) extended the minimum structure method of Georgoulis, LaBonte, and Metcalf (2004) to the problem of velocity determination, in a method they termed minimum-structure reconstruction (MSR). Schuck (2005) showed that, formally, LCT is not consistent with the induction equation’s normal component, which can be expressed as a continuity equation; instead, LCT is consistent with the advection equation. Building upon the “differential LCT” (DLCT) method developed by Lucas and Kanade (1981), Schuck (2006) developed the differential affine velocity estimator (DAVE), which employs least-squares fitting to solve the continuity-form of equation (2) for \mathbf{u} and its spatial derivatives (Schuck 2006). All of the methods listed above can be applied to chromospheric as well as photospheric magnetograms.

Flow estimation techniques that explicitly employ equation (2) have been termed “inductive” (Georgoulis and LaBonte 2006); examples include IM, ILCT, MEF, and MSR. Tracking methods, e.g., FLCT, DLCT, and DAVE, use the evolution of structure in B_z to quantify proper motions, and may also be referred to as “optical flow” techniques (Schuck 2006). Tracking techniques usually apply a windowing function, centered on each pixel tracked, to derive the optical flow in the neighborhood of that pixel. Since this window imposes a scale length, tracking methods have been criticized for their selective sensitivity to flows on the imposed window scale (Georgoulis and LaBonte 2006). The tracking techniques mentioned thus far might be termed “Eulerian methods,” as they estimate velocities over a set of pixels from an image pair. In contrast, “feature tracking” techniques (DeForest *et al.* 2007), in which discrete “features” are identified from structure in B_z maps and followed in time, might be termed “Lagrangian” techniques. We will not discuss feature tracking techniques further in this work.

Generally, velocity estimation techniques are susceptible to errors in magnetograms, because changes in the inferred magnetic field, $\partial_t B_z$, are assumed to

arise from flows via equation (2). Simply put, when noise or systematic errors introduce spurious fluctuations δB_z in B_z , spurious velocities are derived. In particular, in regions where $|B_z|$ is small, δB_z due to noise can be on the order of changes ΔB_z due to actual field evolution. For this reason, tracking methods are expected to estimate flows more accurately in regions where $|B_z|$ is large (barring magnetograph saturation effects) than where $|B_z|$ is small.

The recent proliferation of velocity estimation methods led Welsch *et al.* (2007) to test seven routines' ability to reproduce known flows. They extracted several pairs of "synthetic magnetograms" from ANMHD simulations of a rising flux rope in the upper solar convection zone, and used several methods — two LCT codes, DAVE, IM, ILCT, MEF, and MSR — to estimate flows responsible for magnetic evolution between each pair. They then compared properties of the estimated flows with those of the "true" flows from the MHD code. (These flow reconstructions were not blind: those deriving flow estimates had access to the true flow.) They found that MEF, DAVE, FLCT, IM, and ILCT performed similarly by many measures, but that MEF estimated the fluxes of magnetic energy and helicity quite well. The other methods tested estimated the fluxes of magnetic energy and helicity through the magnetogram layer poorly.

While the MHD simulations of field evolution in the solar interior used by Welsch *et al.* (2007) did not accurately model photospheric field evolution, they did provide a valuable tool for testing velocity estimates. In the near future, blind tests, with simulated data that more accurately model photospheric field evolution, are planned, as are tests of the sensitivity of flow estimation methods to noise. (Application of these methods to synthetic chromospheric vector magnetograms will also be investigated.)

3. Theoretical considerations

As noted in the discussion of equation (2), $\partial_t B_z$ alone cannot fully specify the three components of \mathbf{v} . We note that both evolution in \mathbf{B} (equation [1]) and the ideal, upward fluxes of magnetic energy S_z (Démoulin and Berger 2003),

$$S_z = \frac{1}{4\pi} \int dA' \hat{\mathbf{z}} \cdot [(\mathbf{v} \times \mathbf{B}) \times \mathbf{B}] = \frac{1}{4\pi} \int dA' (\mathbf{u} B_z) \cdot \mathbf{B}_h, \quad (4)$$

and magnetic helicity (Démoulin and Berger 2003; see also Pariat *et al.* 2005)

$$dH_A/dt = 2 \int dA' \hat{\mathbf{z}} \cdot [\mathbf{A}_P \times (\mathbf{v} \times \mathbf{B})] = -2 \int dA' (\mathbf{A}_P \cdot \mathbf{u}) B_z \quad (5)$$

are all linear in $(\mathbf{v} \times \mathbf{B})$. (In equation [5], $\nabla_h = [\partial_x, \partial_y, 0]^T$, $\hat{\mathbf{z}} \cdot \nabla_h \times \mathbf{A}_P = B_z$ and $\nabla_h \cdot \mathbf{A}_P = \hat{\mathbf{z}} \cdot \mathbf{A}_P = 0$.) This dependence means that flows along the magnetic field, v_{\parallel} , do not lead to any evolution in \mathbf{B} , and do not transport either magnetic energy or magnetic helicity across the magnetogram surface. Hence, the components of \mathbf{v} perpendicular to \mathbf{B} ,

$$\mathbf{v}_{\perp} \cdot \mathbf{B} = 0, \quad (6)$$

are of practical interest for most applications of velocity estimation. This equation, combined with equation (2), now provides two equations for the three unknown components of \mathbf{v} .

In this section, we briefly consider possible remedies to the remaining underdetermination, as well as its implications.

3.1. Can Doppler data determine surface magnetic flows directly?

Doppler measurements of the velocity of the magnetized plasma, best determined from Stokes V , Q , and/or U profiles (not I ; see Chae *et al.* [2004]), cannot fully determine whether the inferred plasma flows lie either parallel to or perpendicular to the magnetic field if $B_{\text{LOS}} \neq 0$. This degeneracy is illustrated schematically in Figure 1.

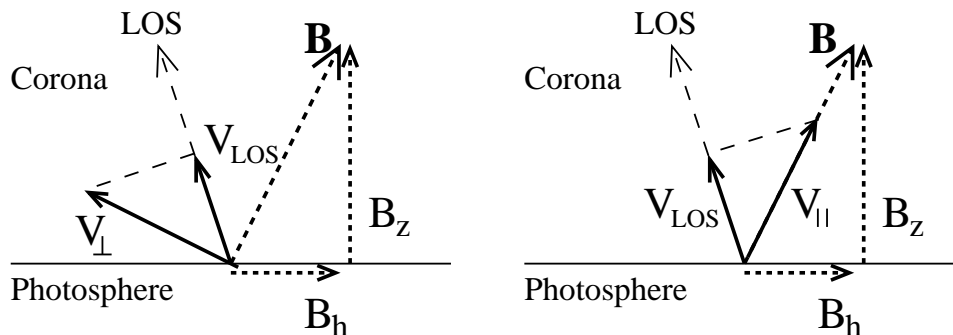


Figure 1. When $B_{\text{LOS}} \neq 0$, a flow \mathbf{v}_{\perp} perpendicular to \mathbf{B} can produce the same LOS velocity as a flow \mathbf{v}_{\parallel} parallel to \mathbf{B} . This means LOS flows inferred from Doppler shifts are insensitive to the relative orientation of \mathbf{v} and \mathbf{B} . Flows parallel to \mathbf{B} do not lead to evolution in \mathbf{B} , and do not transport magnetic energy or helicity. The evolution of B_z at the photosphere, however, can be used to estimate \mathbf{v}_{\perp} . The presence of a field component perpendicular to the page (neglected in this figure) would not affect this analysis.

Doppler shifts do unambiguously determine the perpendicular flow when $B_{\text{LOS}} = 0$. Near disk center, this is approximately satisfied along polarity inversion lines, where B_z changes sign, as noted by (Chae *et al.* 2004) and (Lites 2005). Doppler observations have shown that some polarity inversion lines can also be velocity inversion lines (Deng *et al.* 2006), which can be interpreted as the manifestation of siphon flows moving along field lines that arch over the polarity inversion line.

Doppler measurements can, however, be combined with an estimate of the perpendicular velocity \mathbf{v}_{\perp} from one of the techniques described above to recover the flow parallel to the magnetic field: subtracting the projection of \mathbf{v}_{\perp} onto the LOS from v_{LOS} gives the LOS component of v_{\parallel} , which can be divided by the cosine of the angle between \mathbf{B} and the LOS to give v_{\parallel} . Georgoulis and LaBonte (2006) have employed this approach in an observational study of active region flows, and Ravindra and Longcope (2007) have investigated the use of Doppler shifts in a theoretical study using the data from Welsch *et al.* (2007).

In the following discussion, any reference to \mathbf{v} should be assumed to refer to \mathbf{v}_{\perp} .

3.2. Inductive flows

One can employ a Helmholtz decomposition of equation (3),

$$\mathbf{u}B_z = \mathbf{v}_h B_z - v_z \mathbf{B}_h = -\nabla_h \chi - \nabla_h \times \psi \hat{\mathbf{z}}, \quad (7)$$

to express $\mathbf{u}B_z$ in terms of “inductive” and “electrostatic” potentials (Longcope 2004) χ and ψ , respectively. (We note that, assuming the ideal Ohm’s Law, these potentials can be expressed as sources of a horizontal electric field,

$$\mathbf{E}_h = c^{-1}(\hat{\mathbf{z}} \times \mathbf{u}B_z) = c^{-1}(\nabla_h \times \chi \hat{\mathbf{z}}) - c^{-1} \nabla_h \psi .) \quad (8)$$

Inserting equation (7) into equation (2) yields a Poisson equation for χ ,

$$\partial_t B_z = \nabla_h^2 \chi, \quad (9)$$

meaning the evolution of B_z between a pair of sequential magnetograms, $\Delta B_z / \Delta t$, specifies χ . This does not, however, constrain ψ in any way.

Equation (9) can be solved to determine the purely inductive flux transport rate, i.e., one that assumes $\psi = 0$,

$$\mathbf{u}_I B_z = -\nabla_h \chi, \quad (10)$$

where the subscript I denotes that the flux transport velocity is inductive. In principle, equation (10) can be substituted into equation (3) and combined with equation (6) to determine \mathbf{v} . In practice, though, solving this system of equations for \mathbf{v} requires division by B_z , which weights regions of weak $|B_z|$ more strongly than regions of large $|B_z|$, and, as discussed in §1., flows are expected to be poorly estimated in such regions. For some applications, however, an estimate of $\mathbf{u}B_z$ is sufficient; for instance, equations (4) and (5) imply that $\mathbf{u}B_z$ can be used to estimate the fluxes of magnetic energy and helicity into the corona without determining \mathbf{v} .

The ANMHD data used by Welsch *et al.* (2007) can be used to demonstrate the ability to estimate flow properties from the induction equation alone. In Figure 2, we show a snapshot of the magnetic (grayscale background for B_z and white vectors for \mathbf{B}_h) and velocity (black/white contours for v_z , and black arrows for \mathbf{v}_h) fields in a cross section of the simulation domain near the top of the convection zone. We note that the strong fields present (~ 8000 G) are appropriate to the high- β solar interior, but are substantially stronger than observed photospheric field strengths. These data are described in much greater detail in Welsch *et al.* 2007 (Welsch *et al.* 2007).

Using the ΔB_z between two synthetic magnetograms 125 seconds before and after the magnetogram shown in Figure 2, we solved equation (9) with a Fourier technique to compute $\mathbf{u}_I B_z$. Figure 3 shows a scatter plot comparing ANMHD’s flux transport rate, $\mathbf{U}_I B_z$, with $\mathbf{u}_I B_z$, along with the linear correlation coefficients for the x and y components. These correlation coefficients compare quite favorably with results of the tests by Welsch *et al.* (2007). We also computed a least-absolute-difference linear fit of $|\mathbf{u}_I B_z|$ as a function of $|\mathbf{U}_I B_z|$, and found a slope of 0.4, when 1.0 would be ideal; evidently, inductive flux displacements underestimate ANMHD’s true flux displacements.

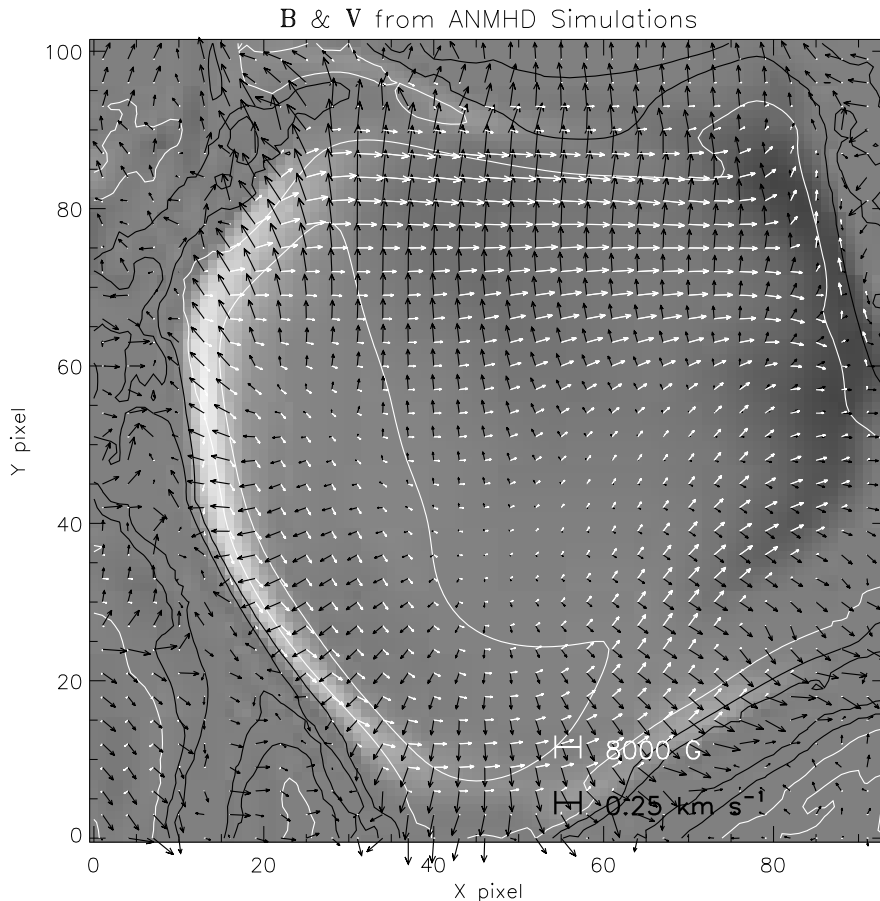


Figure 2. A snapshot of the magnetic and velocity fields in a cross section of an ANMHD simulation of a flux rope rising through the convection zone, extracted from near the top of the domain. The grayscale background shows B_z , white vectors show \mathbf{B}_h , black (white) contours show smoothed downflows (upflows) of v_z , and black arrows show \mathbf{v}_h . Only components of \mathbf{v} perpendicular to \mathbf{B} are shown.

In addition, we calculated the estimated fluxes of magnetic energy and magnetic helicity, separately trying the methods of Démoulin and Berger (2003) and Pariat *et al.* (2005) for the helicity flux. We found that $\mathbf{u}_I B_z$ determined by our Fourier method recovered 30% of the energy flux, but only 10% of the helicity flux. If, however, the estimated helicity flux was summed only over strong-field pixels — in which $|B_z|$ exceeded 5% of $\max(|B_z|)$ — the Démoulin and Berger (2003) approach recovered 20% of the helicity flux from all pixels, while the Pariat *et al.* (2005) approach recovered 15% of the helicity flux from all pixels. While these results compare favorably with most of the velocity estimation methods tested by Welsch *et al.* (2007), they reveal that inductively determined flux transport rates lack essential information about the fluxes of energy and helicity — presumably related to ψ being unconstrained by equation (9).

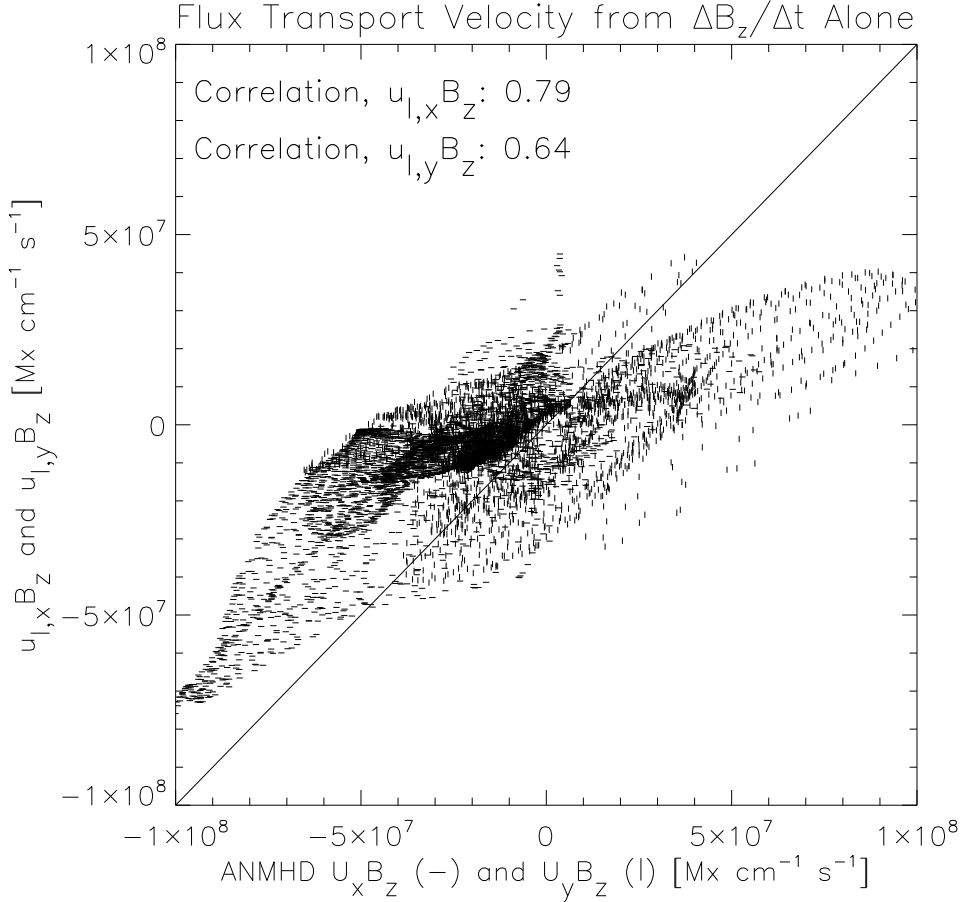


Figure 3. A scatter plot comparing ANMHD’s flux transport rate, $\mathbf{U}_I B_z$, with that derived from equation (9), $\mathbf{u}_I B_z$, along with the linear correlation coefficients for the x and y components. The solid line is not a fit; it is the desired slope, and is shown to emphasize departures from that slope.

The inductive potential χ used in these test was determined with a Fourier technique, which assumes periodicity, and solves for χ on all pixels, including those with weak vertical field. We ran the same tests with an alternative potential function, χ' , which satisfies homogeneous boundary conditions over a masked region that includes only pixels with $|B_z| > 170$ G. Derived by B. Ravindra and D.W. Longcope, χ' was used for the inductive component of MEF flows in the tests conducted by Welsch *et al.* (2007). We found that, compared to flux transport rates from χ , flux transport rates derived from χ' were more poorly correlated with ANMHD’s flux transport rates, underestimated $|\mathbf{U}B_z|$ more severely, and recovered less of the vertical fluxes of magnetic energy and helicity. We note that MEF overestimated $|\mathbf{U}B_z|$ in the tests performed by Welsch *et al.* (2007). This implies that the superior performance of the MEF approach at estimating fluxes of magnetic energy and helicity in Welsch *et al.* (2007) derives from MEF’s specification of ψ .

3.3. Sensitivity of flow estimation to $\nabla_h B_z$

As Démoulin and Berger (2003) observed, the underdetermination of \mathbf{v} by equation (2) implies that there exists a class of flows that cause no evolution in B_z , but that can inject large amounts magnetic energy and helicity. Flows that do not alter B_z satisfy

$$\mathbf{v}_{h,0}B_z - v_{z,0}\mathbf{B}_h = \mathbf{u}_0B_z = -\nabla_h \times \psi \hat{\mathbf{z}} . \quad (11)$$

Because these flows lie in the null space of equation (2), we call them “null flows,” and denote them with a zero subscript. While flows along contours of B_z — “contour flows” — are a well known subset of null flows, modelers have employed other null flows; see, e.g., (Lynch *et al.* 2005).

Taking the curl of equation (7) yields

$$\nabla_h \times \mathbf{u}B_z = \nabla_h^2 \psi . \quad (12)$$

A flux transport velocity, $\mathbf{u}^{(EST)}$, estimated from any optical flow technique (e.g., DAVE or FLCT) can be used with (12) to find ψ , and equation (9) to find χ . This is the essence of ILCT (Welsch *et al.* 2004); but it goes a step further, and uses equations (7) and (6) to determine \mathbf{v} . Since, however, optical flow techniques ultimately depend on $\Delta B_z / \Delta t$, and flows associated with ψ do not alter B_z , this procedure is expected to be insensitive to such flows.

We can use FLCT flows to illustrate the difference in sensitivity of one velocity estimation technique to flows along contours of B_z versus flows along gradients of B_z . In Figure 4, we plot selected contours of ANMHD’s average B_z over a grayscale image of the change ΔB_z over the same 250 second time interval used to estimate $\mathbf{u}_I B_z$ in §3.2. We also plot ANMHD’s instantaneous flux displacement, $\mathbf{U}B_z$, decomposed into components along contours (gradients) of B_z with white (black) vectors. Flow estimation techniques that depend upon $\partial_t B_z$ are expected to be insensitive to flows that transport flux along contours of B_z (white vectors).

Using \mathbf{u} from FLCT in equation (12) to find ψ , and equation (7) to combine χ from equation (9) with ψ , we attempted to reconstruct ANMHD’s flux displacement, $\mathbf{U}B_z$, from Figure 4. In Figure 5, we show scatter plots of flux displacements from ANMHD and our estimates of these (denoted $\mathbf{U}B_z$ and $\mathbf{u}B_z$, respectively) along $\nabla_h B_z$ (horizontal dashes) and contours of B_z (vertical line segments). Flows along $\nabla_h B_z$ are recovered more accurately than flows along contours of B_z , as quantified by the linear correlation coefficients shown on the plot. The fact that contour flows are even partially recovered presumably results from variations in the spatial structure of B_z in the neighborhood of each tracked pixel.

4. Discussion

We have briefly reviewed central concepts regarding surface flow estimation from magnetograms. In addition, we have presented the results of simple tests which demonstrate that the induction equation’s normal component, equation (2), can be used to quantitatively estimate flux transport rates. Fluxes of magnetic energy and helicity derived from these estimates are, however, likely to possess

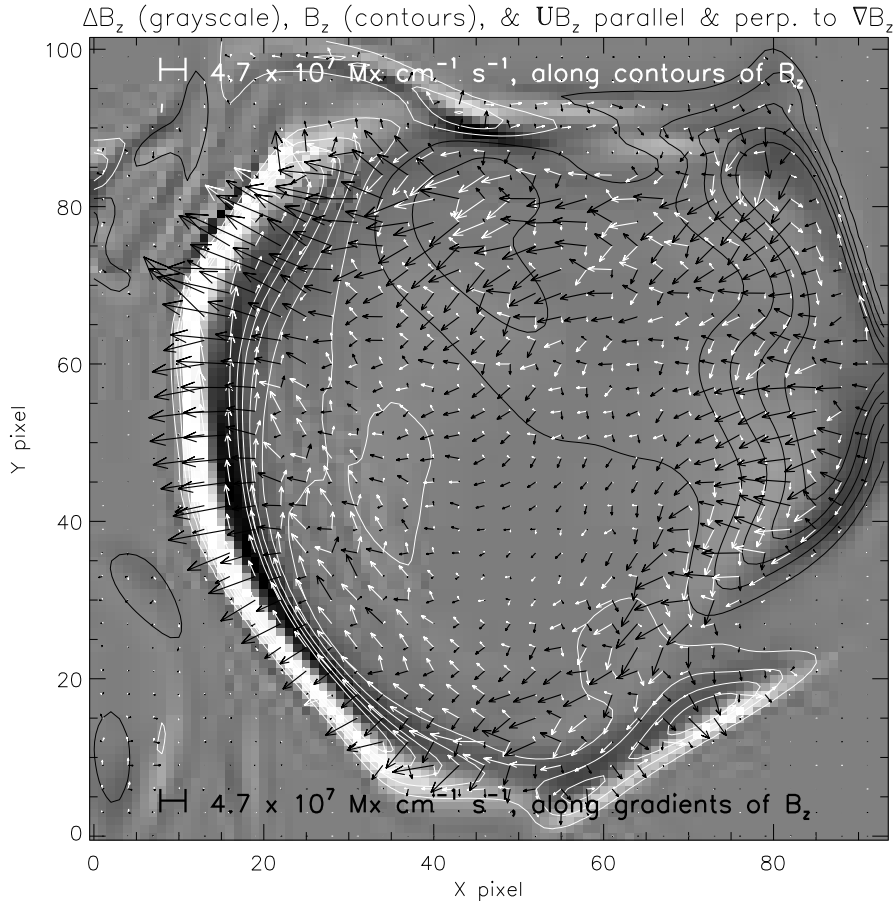


Figure 4. The change ΔB_z in the normal magnetic field is shown in grayscale, along with selected contours of B_z (white for $B_z > 0$, black for $B_z < 0$). ANMHD's instantaneous flux displacement, $\mathbf{u}B_z$, decomposed into components along contours (white vectors) and gradients (black vectors) of B_z , is overplotted. Flow estimation techniques that depend upon $\partial_t B_z$ are insensitive to flows that transport flux along contours of B_z (white vectors).

significant systematic errors. We have also demonstrated that flow estimation techniques that depend upon evolution in B_z alone are insensitive to flux transport along contours of B_z , compared to flux transport along $\nabla_h B_z$. Equations (4) and (5), which depend on the dot products of $\mathbf{u}B_z$ with \mathbf{B}_h and with \mathbf{A}_P respectively, combined with the sensitivity of $\mathbf{u}B_z$ to $\nabla_h B_z$, suggest that if \mathbf{B}_h and/or \mathbf{A}_P lie primarily along $\nabla_h B_z$, then the fluxes of magnetic energy and/or helicity can, in principle, be recovered accurately from $\Delta B_z / \Delta t$. If, in contrast, \mathbf{B}_h and/or \mathbf{A}_P lie primarily along contours of B_z , then the fluxes of magnetic energy and/or helicity probably cannot be recovered accurately from evolution in B_z alone.

We note that, as discussed in (Welsch *et al.* 2007), the ANMHD data used in the tests presented here differ from actual magnetograms in significant ways,

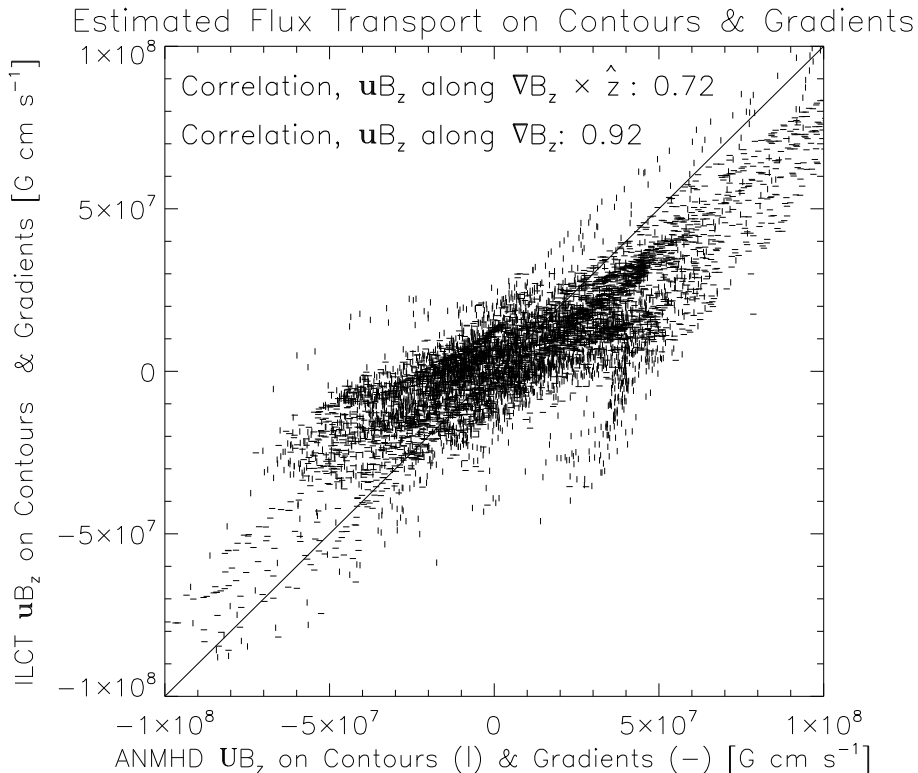


Figure 5. Scatter plots of ANMHD’s UB_z and estimated uB_z are shown. The vectors have been decomposed into components along gradients in B_z (plotted with -) and contours of B_z (plotted with |). Flux transport along gradients of B_z is recovered more accurately than transport along contours of B_z , as quantified by the linear correlation coefficients shown for each component. The solid line is not a fit; it is the desired slope, and is shown to emphasize departures from that slope.

so the properties of flows estimated from actual magnetograms will probably differ substantially from the properties of flows estimated from ANMHD data.

Acknowledgments. Data from MEF velocity estimates were courtesy of B. Ravindra and D. W. Longcope. We acknowledge support from grant NNG05G144G-04/08, from NASA’s Sun-Earth Connections Theory Program.

References

- Chae, J. 2001, *ApJ* 560, L95.
 Chae, J., Moon, Y., and Pevtsov, A. A. 2004, *ApJ* 602, L65.
 Démoulin, P. and Berger, M. A. 2003, *Sol. Phys.* 215, 203.
 DeForest, C. E., Hagenaar, H. J., Lamb, D. A., Parnell, C. E., and Welsch, B. T. 2007, *ApJ* in press.
 Deng, N., Xu, Y., Yang, G., Cao, W., Liu, C., Rimmele, T. R., Wang, H., & Denker, C. 2006, *ApJ*, 644, 1278
 Georgoulis, M. K. and LaBonte, B. J. 2006, *ApJ* 636, 475.

- Georgoulis, M. K., LaBonte, B. J., and Metcalf, T. R. 2004, ApJ 602, 446.
- Henney, C. J., Keller, C. U., Jones, H. P., and SOLIS Team 2002, Stokes Inversion Techniques for the SOLIS-VSM, in *American Astronomical Society Meeting 200*, #55.14, p. #55.14.
- Kusano, K., Maeshiro, T., Yokoyama, T., and Sakurai, T. 2002, ApJ 577, 501 .
- Leka, K. D. and Metcalf, T. R. 2003, Sol. Phys. 212, 361.
- Lites, B. W. 2005, ApJ, in press —, .
- Longcope, D. W. 2004, ApJ 612.
- Lucas, B. D. and Kanade, T. 1981, An iterative image registration technique with an application to stereo vision., in Hayes, J. P., editor, *Proceedings of the 7th International Joint Conference on Artificial Intelligence (IJCAI 81)*, pp. 121–130, Los Altos, CA, William Kaufmann.
- Lynch, B. J., Antiochos, S. K., de Vore, C. R., and et al. 2005, The Breakout Model for CME Initiation in 3-Dimensions, in *ESA SP-592: Solar Wind 11/SOHO 16, Connecting Sun and Heliosphere*, volume 16.
- Metcalf, T. R., Leka, K. D., and Mickey, D. L. 2005, ApJ 623, L53.
- November, L. and Simon, G. 1988, ApJ 333, 427.
- Pariat, E., Démoulin, P., and Berger, M. A. 2005, A&A 439, 1191.
- Ravindra, B. and Longcope, D. W. 2007, in preparation.
- Scherrer, P. and The HMI TEAM 2005, AGU Spring Meeting Abstracts , A5+.
- Schuck, P. W. 2005, ApJ 632, L53.
- Schuck, P. W. 2006, ApJ 646, 1358.
- Tarbell, T. D. 2006, The Focal Plane Package of the Solar Optical telescope on Solar B, in *AAS/Solar Physics Division Meeting*, pp. #36.02–+.
- Welsch, B. T. 2006, ApJ 638, 1101.
- Welsch, B. T., Fisher, G., and Abbett, W. 2004, ApJ 610, 1148.
- Welsch, B. T., Abbett, W. P., DeRosa, M. L., Fisher, G. H., Georgoulis, M. K., Kusano, K., Longcope, D. W., Ravindra, B., and Schuck, P. W. 2007, ApJ, submitted , <http://solarmuri.ssl.berkeley.edu/~welsch/public/manuscripts/Shootout/MaxMil/ms.pdf>.